Spatially Distributed Water Fluxes in an Andisol under Banana Plants: Experiments and Three-Dimensional Modeling

Julie Sansoulet,* Yves-Marie Cabidoche, Philippe Cattan, Stéphane Ruy, and Jirka Šimůnek

Water fluxes in the subsurface of forested and agricultural ecosystems vary spatially across wide ranges because of several interconnected phenomena. On the one hand, subsurface environments are often highly heterogeneous. On the other hand, infiltration water is often distributed unevenly due to aboveground interception and redistribution of rainfall by the plant canopy. These phenomena have important hydro-ecological consequences because they significantly affect groundwater recharge and nutrient leaching. Field experiments involving subsurface lysimeters and tensiometers were performed to quantify the spatial distribution of fluxes in an Andisol under a banana plant (*Musa acuminata* Colla). Wick lysimeters were installed at a depth of 70 cm at several locations with respect to the banana stem to measure the spatial distribution of subsurface water fluxes. Collected experimental data were simulated using the HYDRUS software package, which numerically solves the Richards equation describing three-dimensional variably saturated water flow in the subsurface. Spatially distributed drainage fluxes were well reproduced with the numerical model. Due to the impact of stemflow, drainage volumes under the banana stem were up to six times higher than in the row downstream from the stem, as well as between rows, as these areas were sheltered from direct rainfall by the banana leaves and received only throughfall.

W ATER FLUXES above and in the soil exert a major effect on solute transport in the subsurface and thus significantly influence the quality of subsurface water resources. In the humid tropics, high rainfall amounts significantly exceed the potential evapotranspiration from the soil–plant–atmosphere system. Consequently, drainage is the main component of the subsurface water balance. Water fluxes in the subsurface of forested and agricultural ecosystems vary spatially across wide ranges because of several interconnected phenomena. While on the one side the subsurface environment is often highly heterogeneous, on the other side infiltration water is often distributed unevenly due to aboveground interception and redistribution of rainfall by the plant canopy. Part of the rainfall water intercepted by plant leaves

J. Sansoulet and Y.-M. Cabidoche, Inst. National de la Recherche Agronomique, Unité Agropédoclimatique de la Zone Caraïbe, Domaine Duclos, 97170 Petit-Bourg, Guadeloupe, France; P. Cattan, Centre International de Recherche Agronomique pour le Développement, Unité Systèmes de Culture Bananes, Plantains et Ananas, Station Neufchâteau, 97130 Capesterre Belle Eau, Guadeloupe, France; S. Ruy, Inst. National de la Recherche Agronomique, Unité Climat-Sol-Environnement, Domaine Saint-Paul, Site Agroparc, 84914 Avignon, France; J. Šimůnek, Dep. of Environmental Sciences, Univ. of California, Riverside, CA 92521. Received 13 Apr. 2007. *Corresponding author (juliesansoulet@yahoo.fr).

evaporates back to the atmosphere, part falls onto the soil surface between leaves (throughfall), and part flows around branches and stems downward toward the soil surface (stemflow).

Stemflow is an important hydro-ecological process in forested and agricultural ecosystems because it results in a spatially localized input of water into the soil at the foot of the plant stem and thus significantly influences groundwater recharge (Taniguchi et al., 1996). Many catchment and subcatchment studies concerned with the effect of agricultural and forest covers on the distribution of water at the soil surface have therefore partitioned the incident gross precipitation into stemflow and throughfall at the plant scale (Levia and Frost, 2003). Due to their large leaves, banana crops exhibit a strong partitioning of rainfall, resulting in a high amount of stemflow (Bassette and Bussière, 2005). As a consequence, stemflow appears to be the primary cause of the spatial distribution of drainage. Moreover, banana plants are often locally and intensively fertilized at the foot of the plant stem with up to 400 kg N ha^{-1} yr^{-1} and 800 kg K ha^{-1} yr^{-1} (Godefroy and Dormoy, 1988). Stemflow is thus likely to remove large quantities of these nutrients from the root zone and leach them into the deeper subsurface.

Extensive literature has been produced about rainfall interception in forested ecosystems (Carlyle-Moses and Price, 1999) and about the spatial variability of subsurface drainage due to different types of irrigation (Young and Wallender, 2002) and plant evapotranspiration (Arya et al., 1975). Still, few studies have been performed to quantify the effect of stemflow on the spatial pattern of drainage and associated solute leaching (Sansoulet et al., 2007). Recent lysimetric data have shown a strong influence of

the vegetation structure on gravitational drainage, which occurs mainly below the stem of a banana crop (Cattan et al., 2007). The researchers underlined the difficulty in measuring drainage using coupled atmospheric and wick lysimeters. While atmospheric lysimeters exhibit percolation only under saturated conditions, wick lysimeters often overestimate water fluxes because of the induced suction.

Numerical models have, during the last 25 yr, increased our understanding of drainage processes in soil–plant–atmosphere systems (Jarvis, 1991; Lafolie, 1991; Šimůnek et al., 2006). Two essential factors must be addressed when modeling water flow through the soil under banana plants: (i) three-dimensional water flow has to be modeled at the scale of the plant, considering the row and interrow phenomena; and (ii) the spatial distribution of rainfall due to its interception and redistribution under the banana plant has to be evaluated. It thus appears that a distributed approach with spatially distributed boundary conditions and soil hydraulic properties is probably the most appropriate to address this problem. The use of a distributed model makes it possible to determine the system response at each point of the domain and to identify the critical areas, such as the domain under the banana stem, that are likely to contribute most to the drainage.

Models simulating water flow in the vadose zone differ in their conceptual approach, complexity, and mathematical formulation. For a complete review of water flow models, see Herbst et al. (2005). Among the large number of well-established modeling programs, HYDRUS (Šimůnek et al., 2006) was selected because it allows application of the different boundary conditions required for this problem (e.g., stemflow, throughfall, free drainage, and seepage face), has a sophisticated graphical user interface that simplifies the design of complicated three-dimensional geometries of the transport domain, enables consideration of different soil layers and their inclination, considers root water uptake, distinguishes between soil evaporation and plant transpiration, and also simulates solute movement. An extensive literature exists (www.pc-progress.cz/Pg_Hydrus_References.htm; verified 8 Apr. 2008) documenting the usefulness of HYDRUS models (one, two, or three dimensional) to simulate plant water uptake (Chabot et al., 2002; Sommer et al., 2003), to evaluate surface runoff (Mertens et al., 2001), to predict groundwater table fluctuations (Ventrella et al., 2000), to analyze flow in the vadose zone above the groundwater table (Kao et al., 2001), to evaluate pesticide transport through the soil (Persicani et al., 1995; Pang et al., 2000), to assess the effects of irrigation on the spatial distribution of drainage (Assouline, 2002), and for many other purposes. Still, no three-dimensional modeling study has been performed to evaluate the effect of rainfall distribution under plants on water flow in soils.

This study was an extensive field study undertaken to evaluate distributed subsurface water fluxes under banana plants and to use the collected data to evaluate and numerically simulate these distributed water fluxes using the HYDRUS software package. Hence, the study had several phases: (i) laboratory experiments to obtain soil hydraulic parameters characterizing the unsaturated hydraulic conductivity function, $K(h)$, and the soil water retention curve, $\theta(h)$; (ii) field experiments to measure surface water fluxes (stemflow and throughfall) and subsurface pressure heads and drainage fluxes; and (iii) numerical modeling using the HYDRUS model to predict distributed water fluxes and compare them to the in situ drainage measurements.

Materials and Methods

Field Experiments

In the French West Indies, intensive banana cultivation on volcanic ash soils has been going on since the 1960s (Ndayiragije, 1996). These soils, particularly the Andisols (Soil Survey Staff, 1996), are well known to have a high infiltration capacity. Consequently, banana plantations represent a large source of nonpoint-source pollution endangering subsurface groundwater resources. From 15 June to 29 Nov. 2004 (168 d), field experiments with installed lysimeters and tensiometers were performed to quantify the spatial distribution of drainage fluxes in an Andisol after rainfall interception by banana plants. The experiments were performed at the CIRAD research facility in Guadeloupe (Basse Terre), French West Indies (16°09′ N, 61°16′ W, 250 m above sea level).

The Andisol from the field site was described by Ndayiragije (1996). It was formed by weathering of quaternary volcanic ash deposits. The silty A horizon (0–40 cm) exhibits a medium, clear, friable structure. The soil aggregates are separated by many tubular pores. The B horizon (40–80 cm) has a fluffy touch and a continued macroscopic structure with medium and fine tubular pores. The hydraulic properties of the Andisol were measured in the field as well as in the laboratory. Soil property measurements (organic C, bulk density, and total porosity) were performed at the laboratory of the INRA Agropedoclimatic Unit, Guadeloupe, French West Indies.

The experimental field was a small watershed of 6000 m^2 with an average slope of 12%. Planting of the banana plants (1800 plants ha^{-1}) took place on 2 Apr. 2003. The experimental period was during the second banana cycle. Rainfall was measured at a 1-min time interval using a tipping bucket rain gauge (ARG100, Campbell Scientific, Logan, UT) with a sensitivity of 0.2 mm per tipping installed at the bottom of the experimental field. The tipping bucket was connected to both a Campbell CR10 datalogger and a global system for mobile communications (SM TC35T, Campbell Scientific) for remote transfer of data. An automated meteorological station was located 500 m from the experimental plot. Global and net radiation, air temperature, relative humidity, and wind speed and direction were measured every 15 s and then averaged and stored for 5-min intervals.

Collection of leachates at different positions relative to the banana plant aimed at the following two objectives: (i) apprehending local variations of water fluxes relative to the redistribution of rainfall by banana foliage (stemflow and throughfall); and (ii) taking into account the zone influenced by the stemflow and how the stemflow is redistributed with respect to the direction of the slope.

Five experimental plots were instrumented in June 2003. The first site was upslope of the field where the A horizon was 10 cm thinner (due to tillage erosion), two were downslope of the field where the soil accumulated, and two were in the middle of the field. One of the plots, called the *fully equipped plot*, was isolated from the neighboring soil with a metal sheet and equipped with a runoff collector (Fig. 1) and a stemflow collector (installed at the stem of the banana plant). While 8% of the stemflow flux was stored in the partitioner, the remaining 92% was reinjected
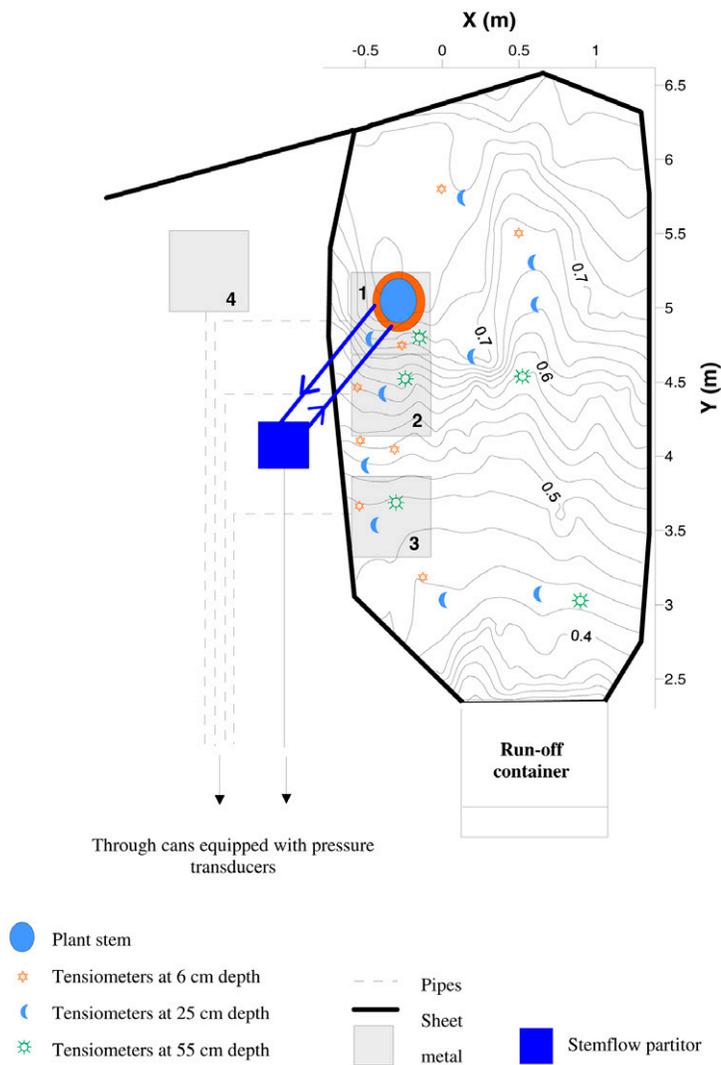
FIG. 1. Schematic representation of the flow domain in the banana plantation with indicated locations of Lysimeters 1 to 4, tensiometers, and the stemflow collector.

at the plant stem. The collectors for drainage, runoff, and stemflow at this site were also equipped with pressure transducers that were linked to the Campbell CR10 datalogger. At the other four plots, soil solution samplers were weighed manually after each rainfall event.

Distributed drainage was measured using glass wick lysimeters. Wick samplers with a fiberglass wick that maintains a fixed tension are the most appropriate and cost-effective devices for collecting the leachate (Boll et al., 1992; Rimmer et al., 1995; Vandervelde et al., 2005). A 45- by 45- by 5-cm steel plate container was first filled with soil from the B horizon. A 2-cm-diameter hole was then drilled in a corner of the bottom plate of the container to insert the 1.45-cm-diameter wick. The upper end of the wick was manually unbraided, frayed, and spread evenly across the soil in the plate. The length of the wick in each lysimeter was calculated according to Lacas et al. (2003). Thirty centimeters of the wick was placed horizontally on the plate. The wick terminated 50 cm below the plate, corresponding to a total height of 55 cm and an air-entry value of –5 kPa in the wick material. The hydrodynamic parameters of the wick were obtained using the experimental data of Knutson and Selker

(1994) and Lacas et al. (2003). At the time of installation, a pit 2 m deep was dug between the plant rows and the sampling container was installed in a 70- by 70-cm horizontal excavation in the vertical face of the soil 30 cm below the A horizon. Each lysimeter was set 30 cm back from the vertical face of the pit and kept in contact with the upper soil, with beams and quoins holding it in place. The soil profile above the lysimeters, including the banana plants, surface litter, the A horizon, the tillage pan and the B horizon, was not disturbed. The wicks were encased in polyethylene pipes set in a trench with 2% slope and connected to a collection of jerry cans 15 m from the experimental plot. Thus, water flowing through the soil was intercepted by the container, drawn into the wick, and conducted to the sampling cans. After installation, the pit and trench were refilled with the original material (B and A horizons).

Each experimental site included four lysimeters that intercepted water at different positions relative to the stem (Fig. 1). Twenty lysimeters were installed overall. Two lysimeters were considered to be affected by stemflow. Lysimeter 1 was located directly below the stem, while Lysimeter 2 was located between 25 and 70 cm downslope from the stem. The third lysimeter (Lysimeter 3) was also located in the row of banana plants between 120 and 165 cm downslope from the stem under the leaves of a neighboring banana plant. This lysimeter was considered to be affected by throughfall and only to a lesser extent by stemflow. The last lysimeter (Lysimeter 4) was installed between two banana plants between rows, 95 cm away from the banana stems.

A series of tensiometers (SKT 850, SDEC, Reignac sur Indre, France), capable of measuring pressure heads between 0 and –99 kPa, were installed in multiple locations at each experimental site. In the fully equipped plot, tensiometers were installed at three depths (6, 25, and 55 cm) above the four lysimeters and around the banana plant (Fig. 1) and the time step for measurements was between 10 s (during rainfall) and 15 min (between rainfalls). At other sites, they were installed at 20-, 40-, and 60-cm depths near the banana stem and downslope from the stem in the row in four sets. Pressure heads were measured every 30 s, then averaged and stored for 15-min intervals. Tensiometers were connected to the same Campbell CR10 datalogger as the tipping bucket.

The topography of the fully equipped plot was measured using a Trimble 3300DR tacheometer (Trimble Geomatics, Dayton, OH). To evaluate the water balance, daily evapotranspiration (ET) before and after banana flowering was calculated during the 168-d experiment according to (i) Pellerin (1986), who expressed the potential evapotranspiration, ET_P, as a function of the global radiation (i.e., $ET_P = 0.23 \times$ global radiation), and (ii) Monteith (1965), who related the actual evaporation to its potential value using the crop coefficients k (i.e., $ET = kET_P$).

Governing Flow Equation

Water flow was simulated using the HYDRUS model (Šimůnek et al., 2006) to numerically solve the Richards equation (Richards, 1931) describing water movement in three-dimensional transport domains in variably saturated porous media. The governing water flow equation is written in a mixed form to

ensure excellent mass balances of the numerical solution (Celia et al., 1990):

$$\frac{\partial \theta}{\partial t} =$$

$$\frac{\partial}{\partial x}\left[K\left(\frac{\partial h}{\partial x}\right)\right] + \frac{\partial}{\partial y}\left[K\left(\frac{\partial h}{\partial y}\right)\right] + \frac{\partial}{\partial z}\left[K\left(\frac{\partial h}{\partial z} - 1\right)\right] - S \quad [1]$$

where θ is the volumetric water content [$L^3 L^{-3}$], h is the pressure head [L], S is a sink term accounting for the root water uptake [T^{-1}], z is the vertical coordinate [L], x and y are the horizontal coordinates [L], t is time [T], and K is the unsaturated hydraulic conductivity [$L T^{-1}$]. The finite-element method is used in HYDRUS to numerically solve the governing partial differential equations.

Soil Hydraulic Properties

HYDRUS, similar to most models that simulate unsaturated water flow in soils, requires knowledge of two nonlinear functions: the unsaturated hydraulic conductivity function, $K(h)$, and the soil water retention curve, $\theta(h)$. Both $K(h)$ and $\theta(h)$ are either unknown, difficult to measure, or relatively uncertain when estimated indirectly from, for instance, pore or particle size distribution. A widely accepted approach is to measure $\theta(h)$ data on relatively small samples under laboratory conditions and then to use fitted retention curve parameters and the pore-size distribution model to predict $K(h)$.

The relations $K(h)$ and $\theta(h)$ are often parameterized using functions proposed by Mualem (1976) and van Genuchten (1980), which are referred to here as van Genuchten (VG) equations:

$$\theta(h) = \frac{\theta_s - \theta_r}{\left(1 + |\alpha h|^n\right)^m} + \theta_r \qquad h < 0 \quad [2]$$

$$\theta(h) = \theta_s \qquad h \geq 0 \quad [3]$$

with

$$m = 1 - \frac{1}{n} \qquad n > 1 \quad [4]$$

and

$$K(h) = K_s S_e^l \left[1 - \left(1 - S_e^{1/m}\right)^m\right]^2 \quad [5]$$

with

$$S_e = \frac{\theta - \theta_r}{\theta_s - \theta_r} \quad [6]$$

where θ_r and θ_s are the residual and saturated water contents [$L^3 L^{-3}$], respectively, α is the inverse of the air-entry value [L^{-1}], n is the pore size distribution index, K_s is the saturated hydraulic conductivity [$L T^{-1}$], S_e is the relative water saturation (dimensionless), and l is the tortuosity factor (dimensionless). An appropriate value for l is still the subject of debate. Earlier studies have set l equal to 0.5 as the best estimate proposed by Mualem (1976).

We used a combination of the field and laboratory experiments to evaluate the soil hydraulic properties. To be able to account for the effects of soil structure, the soil saturated hydraulic conductivity was directly mea-

sured in the field using the double-ring infiltrometer method (Reynolds et al., 2002) applied to both A and B horizons (four replications). From the double-ring experiment, we took the final steady-state infiltration flux from the inner ring and declared it to be K_s. The laboratory evaporation method (e.g., Wind, 1968; Mohrath et al., 1997; Šimůnek et al., 1998) was used to obtain the other soil hydraulic parameters (i.e., θ_r, θ_s, α, and n). During the experiment on undisturbed soil samples (15-cm diameter and 7-cm height), pressure head profiles (four tensiometers) and mean water contents were periodically measured while water was allowed to evaporate from the top of the sample. Measurements were repeated three times on each sample. The four soil retention parameters describing the VG model were then obtained by minimizing the sum of squared differences between the observed and calculated water contents at each measurement time of the laboratory evaporation experiment. The soil hydraulic parameters for both A and B horizons were then used for simulations with the HYDRUS model.

HYDRUS Simulations

Drainage fluxes calculated using the HYDRUS model were validated using the field drainage data between 25 Sept. and 9 Nov. 2004 (46 d) and statistically evaluated. The modeling period, which was shorter than the experimental period, was representative of the wet season during which the main drainage fluxes were recorded. We chose only 46 d to avoid long simulation times, as three-dimensional simulations are still very computationally demanding.

The flow domain and finite element grid (Fig. 2) were defined so that boundary and initial conditions reproduced the in situ
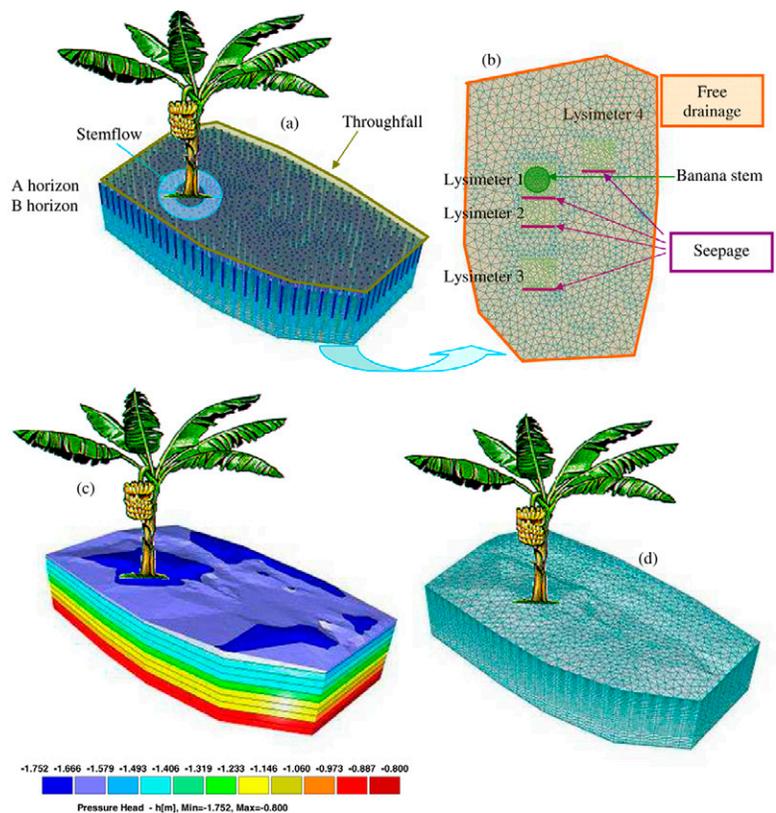
FIG. 2. A schematic representation of the flow domain indicating (a) surface boundary conditions, (b) bottom boundary conditions, (c) pressure head initial conditions, and (d) tetrahedral finite element mesh.

conditions. Water flow in a three-dimensional flow domain with four wick lysimeters (Fig. 2b) was first simulated using HYDRUS. Lysimeter 4 is located outside of the area separated by a metal sheet from the surrounding soil. Since this lysimeter is located exactly in the middle between two banana rows, however, we could use the symmetry between two banana rows and move it into our computational domain on the other side of the banana tree (Fig. 2b). Detailed microtopography measured in the field was used to reproduce the surface conditions. The transport domain was considered to be, on average, 0.7 m deep and the surface area was about 8 m^2. Three different materials with different soil hydraulic properties were defined to account for two soil horizons (A and B) and the wicks. Each soil horizon was assumed to have uniform hydraulic properties. Natural anisotropy was not considered.

Pressure heads measured with tensiometers on 25 Sept. 2004 were used as initial conditions (Fig. 2c). Stemflow and throughfall were used as atmospheric and time-variable flux boundary conditions, respectively, at the soil surface of the domain (Fig. 2a). Throughfall was implemented in the HYDRUS simulation using the time-variable flux boundary condition since the code allows only one atmospheric boundary condition and that one was used for stemflow. It was possible to do that because the new HYDRUS model separates transpiration from the atmospheric boundary condition, unlike previous versions (e.g., HYDRUS-2D). Stemflow measured with the stemflow collector (Fig. 1) was applied on a small area around the plant stem to ensure the proper volume of infiltrating water. Throughfall was then evaluated as the difference between the rainfall volume falling on the area of the fully equipped plot and measured stemflow, divided by the surface area of the plot. As Bassette (2005) has shown, for the banana plants at our experimental site, stemflow increases the incident rainfall relative to the throughfall by 18 to 20 times.

The wicks were simulated using a modified seepage face boundary condition with a limiting pressure of –55 cm to account for the vertical part of the wick. The seepage face is a dynamic outflow boundary condition that changes dynamically according to the flow conditions in the system. HYDRUS assumed a uniform pressure head of –55 cm along the active part of the seepage face through which water seeped out of the wick, and then calculated water flux for this area. Along the inactive segment of the seepage face where water is held in capillaries and cannot seep, the flux across the boundary was assumed to be zero, and the boundary pressure head (lower than –55 cm) was calculated. Free drainage was specified on the remaining part of the bottom of the transport domain (Fig. 2b). This boundary condition represents a unit hydraulic gradient. A zero-flux boundary condition was applied to all vertical boundaries.

Transpiration was simulated using the sink term of Eq. [1]. Roots were assumed to be distributed uniformly both under the plant stem and between the rows in the upper 50 cm of the soil profile (A horizon) according to Lecompte et al. (2003). The water uptake was reduced from its optimal value due to the decrease in the calculated pressure heads according to the model of Feddes et al. (1978).

A finite-element grid (Fig. 2d) was created by first generating two-dimensional triangular elements in the base surface using an automatic grid generator. This two-dimensional grid was then extended in the vertical direction using 20 horizontal layers. The density of the grid was evaluated and judged sufficient when the

numerical solution consistently converged and the water balance error was <1%. High grid densities were generated around the stem, close to the soil surface, at the interface between different soil layers, and close to the wick because the hydraulic gradients could be considerable at these locations at various times. Relatively low grid densities could be used farther away from the wick. The finite-element grid consisted of a total of 33,090 nodes and 184,788 finite elements. Finally, the time discretization was defined using the initial time step of 0.0001 d and the minimum allowed time step of 0.00001 d.

Statistical Evaluation

The model performance was evaluated using all measured and simulated drainage data. The correspondence between observed and predicted soil water drainage fluxes was statistically evaluated using the coefficient of efficiency (E), defined by Nash and Sutcliffe (1970) as

$$E = 1 - \frac{\sum_{i=1}^{n}(\text{observed}_i - \text{predicted}_i)^2}{\sum_{i=1}^{n}(\text{observed}_i - \text{mean}_{\text{obs}})^2} \qquad [7]$$

While calculating the average drainage fluxes at the bottom of the soil profile from spatially variable fluxes is straightforward in the numerical model, it is much more complicated to do from experimental data. In the numerical model, in which fluxes at all locations are known, one can simply add fluxes from different parts of the domain and divide them by the surface area of the domain. In the experimental field, fluxes are measured at only several locations (i.e., lysimeters) and a procedure needs to be devised for evaluating the average drainage flux. The mean drainage flux was calculated in our study from measured fluxes at four lysimeters as a barycentric average relative to the soil surface (Sansoulet et al., 2007) as follows:

$$L_{\text{T}} = \frac{1}{8}\left[L_1 + L_2 + \frac{1}{2}(L_2 + L_3) + L_3 + 4L_4 \right] \qquad [8]$$

where L_{T} is the average value of drainage (mm ha^{-1}) at the field scale, and L_1, L_2, L_3 (row), and L_4 (interrow) are drainage volumes (mm) measured with Lysimeters 1, 2, 3, and 4, respectively.

Results and Discussion

Estimation of Soil Physical and Hydraulic Properties

The physical and chemical properties of the Andisol (Table 1) were in the range expected for Andisols containing allophane (Quantin, 1994). Particularly relevant are the very low bulk density values, the high C content, and the large total porosity considering the large clay content of these soils. Andisols have a soil structure that reflects the abundance of noncrystal-

TABLE 1. Physical properties of the Andisol: clay content, bulk density, organic C, and total porosity.

Horizon	Clay†	Bulk density	Organic C	Total porosity
	%	g cm^{-3}	%	m^3 m^{-3}
A	58.6	0.71	6.69	0.673
B	63.1	0.49	3.73	0.665

† Clay content was determined by quantitative recovery of clay after sonication and dispersion with Na$^+$-saturated resins and before H$_2$O$_2$ oxidation of organic matter.
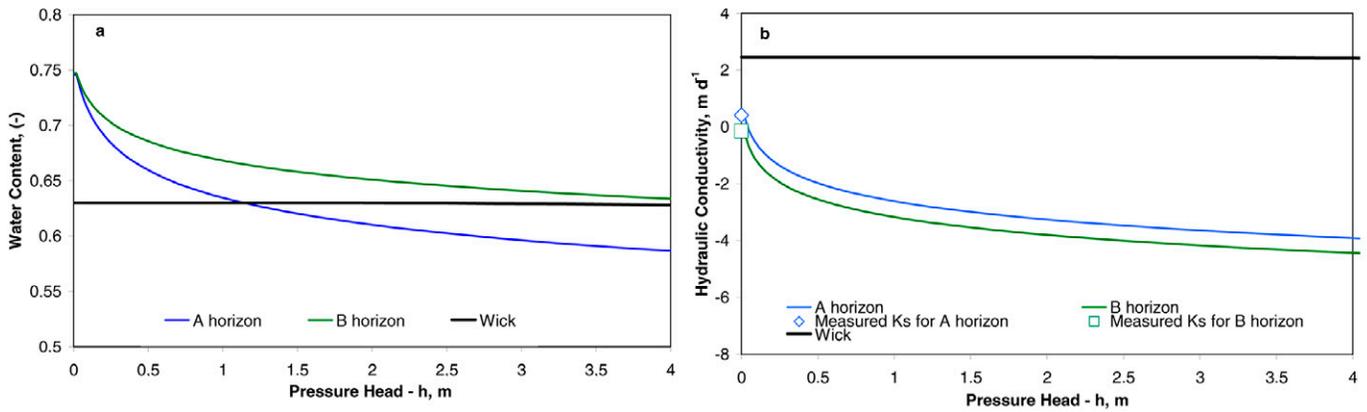
FIG. 3. (a) Soil water retention curves, θ(*h*), and (b) unsaturated hydraulic conductivity functions, *K*(*h*), of two Andisol horizons (A and B) and of the wick.

line materials (Shoji et al., 1993), and thus the entire particle size distribution (silt and sand) is not presented here. Figure 3a shows the soil water retention curves, θ(*h*), for two soil horizons optimized using data from the laboratory evaporation experiments. Since multiple soil samples were used for the evaporation experiments to characterize the retention properties of the soil, several more or less similar retention curves were obtained. A mean curve was fitted for each soil layer (three replicates). The coefficient of determination between measured and fitted water contents ranged between 0.67 and 0.77 for different soil samples. Soil hydraulic parameters for the VG functions for different soil layers are presented in Table 2. Higher variations in retention properties were obtained for the A horizon than for the B horizon. The unsaturated hydraulic conductivity functions, *K*(*h*), were obtained by coupling the results of the laboratory evaporation method and the double-ring infiltrometers (Fig. 3b). Specifically, the Mualem pore size distribution model (Mualem, 1976; van Genuchten, 1980) was used to predict *K*(*h*) from retention curves determined from the evaporation experiments and the saturated hydraulic conductivity determined from the infiltration experiments. It should be noted that the wick could not limit the flow of water in the soil because its hydraulic conductivity is considerably higher than the hydraulic conductivity of either horizon for all pressure heads.

Experimental Results

The annual rainfall (6568 mm) and average temperature (24.1°C) measured in 2004 were quite different from the average values of 3565 mm and 24.4°C collected from 1979 to 1999 by Météo France (2000). During the 168-d experiment, the cumulative rainfall was 4120 mm, with 141 rainfall events with volumes >2 mm. The rain was considered to be an individual rainfall event if the amount of water precipitated during the preceding and following 2 h was <4 mm. The characteristics of these events, given in terms of volume, intensity, and duration, are presented in Fig. 4. A mean rainfall had a volume of 28.2 mm,

a maximum intensity of 96.7 mm h^{-1}, an average intensity of 34.56 mm h^{-1}, and a mean duration of 3 h 46 min, whereas a median rain had a lower volume (9.8 mm) and duration (2 h 6

TABLE 2. Effective soil hydraulic parameters† obtained using the Wind and double-ring infiltrometer methods (direct measurements).

Material	θ_r	θ_s	α	n	K_s	l
	m^3 m^{-3}		m^{-1}		m d^{-1}	
A horizon	0.13	0.75	19.0	1.07	3	0.5
B horizon	0.11	0.75	23.3	1.05	1.06	0.5
Wick	0	0.63	0.06	3.61	280	0.5

† θ_r and θ_s, residual and saturated volumetric water contents; α, inverse of the air-entry value; n, pore size distribution index; K_s, saturated hydraulic conductivity; l, tortuosity factor.
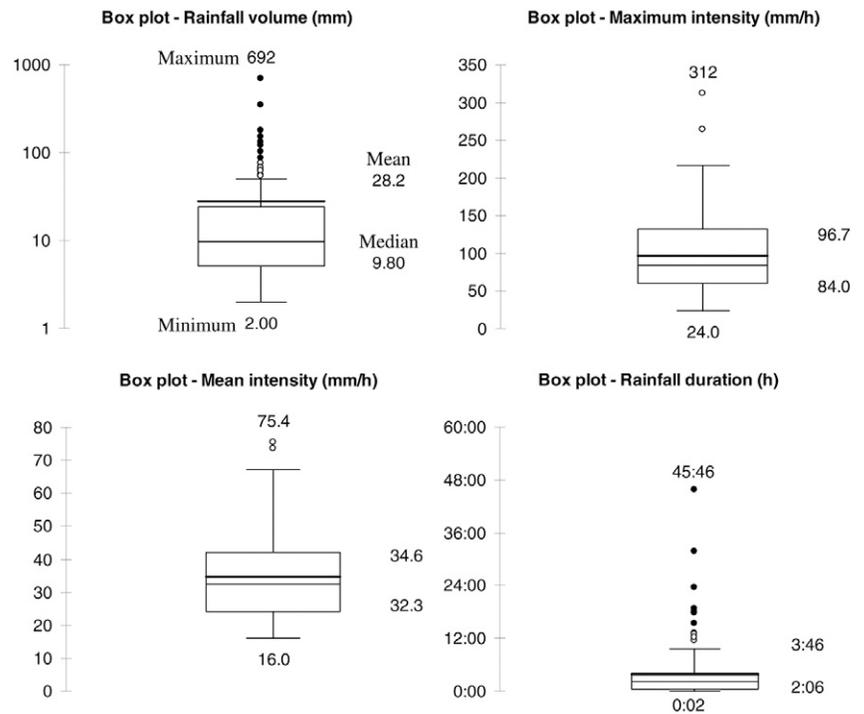
FIG. 4. Box plots characterizing statistical properties of rainfall volume, rainfall duration, and maximum and mean rainfall intensities. Maximum and minimum values as well as first, second, third, and fourth quartiles and mean and median values are plotted.

min) and equivalent intensities. The largest rainfall, which had a volume of 692 mm, maximum intensity of 312 mm h^{-1}, and maximum duration of 45 h 46 min, occurred at the end of the experimental period in November 2004 and was not representative of the other rainfall events.

Measured pressure heads below the plant foot and between the rows at three depths (6, 25, and 55 cm), as well as daily rainfalls, are represented in Fig. 5. Pressure heads recorded below the plant foot are, at all depths, on average about 21% higher than pressure heads recorded between the rows. This is mainly due to higher infiltration at the plant foot because of stemflow. Tensiometers installed closer to the soil surface reacted faster and to a greater extent than those at deeper depth. They were more strongly affected by climatic conditions (rain, evaporation, and transpiration). Pressure heads close to the surface fluctuated between –3.81 and –0.10 m, with an average value of –0.77 m. Pressure heads at 25- and 55-cm depths varied less (from –2.27 to –0.05 m) and were in general higher than at the soil surface, with an average value of –0.55 m, a value very close to the suction exerted by the lysimeter wicks. The higher the rainfall volume, the higher the pressure heads measured. After a rainfall event, the pressure heads increased on average (30 analyzed periods) by 0.34 m at the soil surface, 0.25 m at the 25-cm depth, and 0.16 m at the 55-cm depth. Small rainfall events influenced the pressure heads at deeper depths only very little, explaining why water contents at deeper depths stayed relatively constant, apart from the zone affected by stemflow. Pressure heads measured above Lysimeters 1 and 3 (data not shown) were almost the same as those measured above Lysimeters 2 and 4, respectively.

The observed pressure heads made it possible to discriminate three types of response curves (Fig. 6). The Type 1 curve (not reactive) exhibited little or no variation of pressure heads during and after the rain. The Type 2 curve (fairly reac-
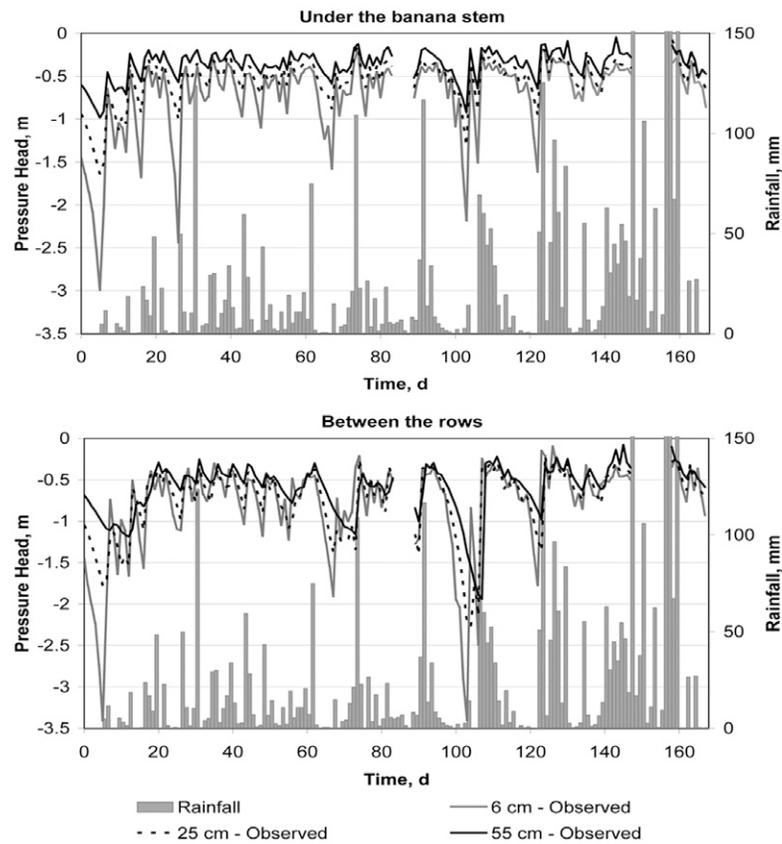
FIG. 5. Mean pressure heads (calculated from five sets, CV = 17%) measured with tensiometers in the soil (top) at the foot of the plant stem (Lysimeter 2) and (bottom) between rows (Lysimeter 4). Precipitation rates are also shown in both figures.
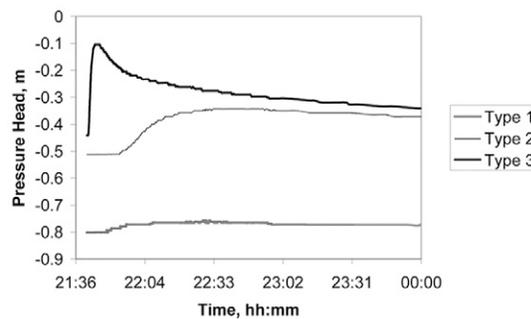
FIG. 6. Typology of the evolutions of pressure heads after a rainfall; *P*, volume of the rainfall event; P1, smallest rainfalls when *P* < 12 mm; P2, moderate rainfalls when *P* is between 12 and 63 mm; P3, highest rainfalls when *P* > 63 mm. The figure also shows the frequency of different response curve types for different depths and rainfall volumes, where Type 1 is not reactive, Type 2 is fairly reactive, and Type 3 is very reactive.
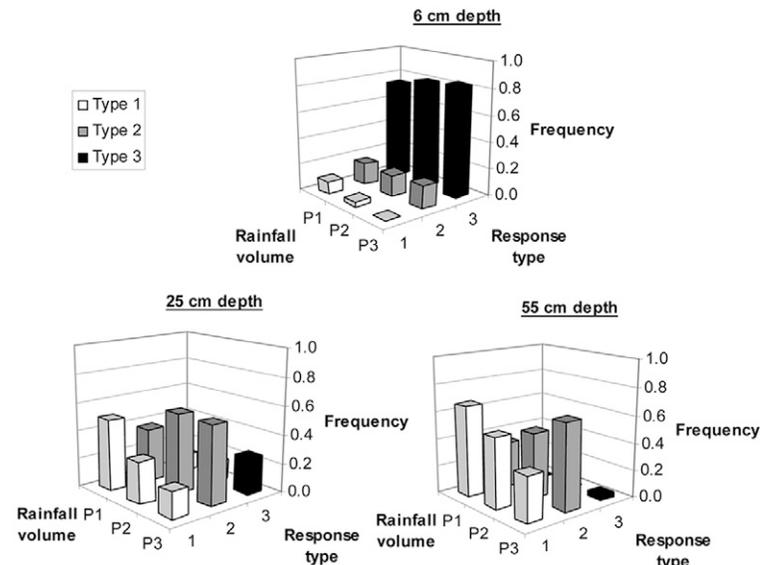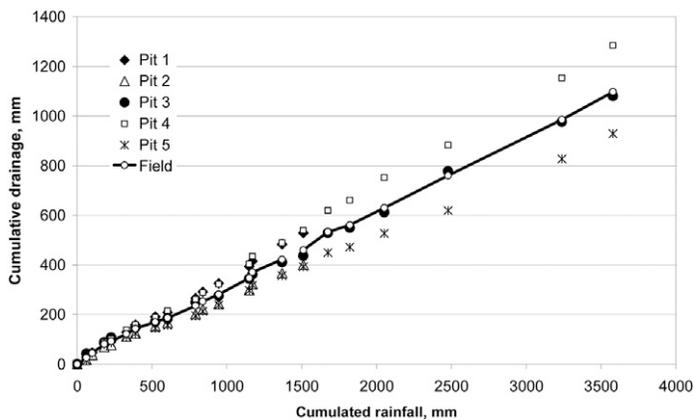
FIG. 7. Comparison of the cumulative rainfall and drainage for five experimental sites. Field = average.

TABLE 3. Components of the mass balance during the 168-d experiment and the 46-d simulated period: water fluxes across the surface (evaporation, rainfall, and surface runoff) and bottom of the soil profile (drainage).

Duration	Rainfall	Drainage	Runoff	Evapotranspiration	Change in storage
		mm			
168 (d)	4120	1808	1709	472	131
46 (d)	1373	539	601	157	76

tive) showed only a small increase and then a very gradual (>5 min) decrease of pressure heads. Finally, the Type 3 curve (very reactive) displayed a fast variation (<5 min) of pressure heads. Type 1 curves made it possible to identify locations or depths that were not affected by the infiltrating water. Type 2 curves represented locations where water flow demonstrated behavior that can be described using Darcy's law (filling of the Andisol micropores and their subsequent draining due to capillary and gravitational forces). The very fast response of pressure heads (Type 3) at some locations was indicative of fast preferential flow through macropores. Histograms (Fig. 6) obtained by analyzing 141 rainfall events show that the majority of responses by tensiometers closest to the soil surface followed the Type 3 curve. This could be partly caused by the disturbance created during installation of shallow tensiometers. Responses of tensiometers installed at deeper depths (25 and 55 cm) usually followed, depending on the rainfall volume, Type 1 and 2 curves. Pressure heads at a 25-cm depth usually followed the Type 2 curve, while those measured at a 55-cm depth followed the Type 1 curve. The higher the rainfall volumes, the more frequent the Type 2 response, and vice versa for the Type 1 response. Type 1 curves appeared mainly in parts of the domain unaffected by stemflow and thus fast percolation of infiltrating water. Tensiometers installed at all depths below the plant foot recorded >85% of responses of Types 2 or 3. This was probably caused by the high amounts of infiltrating water resulting from the stemflow.

The correspondence of measurements from different experimental plots is compared for one time period (27 July–20 Oct. 2004) in Fig. 7. The analyses of the lysimeter data made it possible to evaluate uncertainties related to calculating the average drainage using Eq. [8]. Based on these analyses, Site 3 (the fully equipped plot) was considered representative of the average drainage behavior and was thus subjected to deterministic modeling. Relative uncertainties of the balanced average drainage were 13% when the five sites

were tested (27 July–20 Oct. 2004). These data were considered to be adequate, considering uncertainties related to field lysimeter measurements.

Table 3 summarizes water fluxes at the top (evaporation, infiltration, and runoff) and bottom boundaries (measured drainage) for the 168-d (experimental) and 46-d (computational) time periods. The remainder of the mass balance (i.e., 131 and 76 mm for the 168- and 46-d time periods, respectively) can be attributed to changes in soil water storage and errors associated with measuring or calculating individual fluxes. The largest error is probably associated with calculations of the mean drainage (i.e., Eq. [8]).

HYDRUS Model Simulations and Mass Balance

The total rainfall during the 46-d modeling period was 1367 mm. Pressure heads illustrating the three-dimensional pattern of water flow during a rainfall event under the banana plant are shown in Fig. 8. This figure clearly shows that most of the water

FIG. 8. Pressure heads illustrating the three-dimensional water flow under the banana plant during a rainfall event (total rainfall = 65 mm): (a) 0 d; (b) 1 d; (c) 2 d; (d) 4 d.

flow is concentrated around the stem of the banana tree, while reduced fluxes are apparent downstream from the stem in the row and between the rows.

Figure 9 shows the measured and simulated cumulative drainage fluxes from the four lysimeters vs. time. The mass balance error of the water flow simulation was <1%. Simulations showed that under heavy fluxes, such as those due to stemflow, the wicks reproduced the actual field drainage reasonably well. Mass transfers across the wick–soil interface are determined by differences in pressure heads between the wick and the soil. Under the driest conditions, which corresponded to the lower drainage volumes, pressure heads in the wick were higher than in the soil and the drainage flow stopped. When pressure heads at the bottom of the soil profile decreased below –0.55 m, the flow through the seepage face stopped.

Both measurements and calculations showed relatively fast responses of drainage fluxes in Lysimeters 1 and 2 to rainfall events. Although the overall correspondence between measured and calculated fluxes is very high, there are some distinct differences. While measured drainage in Lysimeters 1 and 2 continued, although at very small rates, even during time periods without rainfall, calculated drainage started and ended rather abruptly and there were long time periods of no calculated drainage. This is because of the type of boundary conditions that were used by the model to represent lysimeters. Lysimeters were modeled using the seepage face boundary condition, which is active when pressure heads exceed the limiting value (–55 cm) and becomes inactive when pressure heads drop below this value.

The numerical model using the measured hydraulic parameters obtained from laboratory and in situ experiments reproduced the general trends of distributed drainage measured using lysimeters under the banana plant fairly well (Fig. 9). Indeed, the comparison of model simulations with field experimental results confirmed that simulated and measured data were quite similar. The model performance was evaluated by comparing the observed and predicted cumulative drainage in Lysimeters 1, 2, 3, and 4 (Fig. 9), as well as observed and predicted pressure heads (Fig. 10) at different soil depths and locations. The coefficient of efficiency (E) ranged from 0.62 to 0.76. The model slightly overestimated fluxes downslope from the plant stem, however. This can be explained by possibly higher root water uptake from deeper soil layers than anticipated. Simulations and collected drained volumes, as well as measured soil pressure heads, demonstrated that the flow under the banana tree was entirely dominated by stemflow and its redistribution in the soil profile. Stemflow infiltrated directly along the plant stem, but part of it was redirected downstream from the stem due to the slope. The drained volumes under the banana stem were six times higher than those downstream from the stem in the row and between the rows since these zones were sheltered by the banana leaves and received essentially only throughfall. Simulations showed that under heavy fluxes, such as those due to stemflow, the wicks reproduced the actual field drainage reasonably well.

Figure 10 presents measured and simulated pressure heads at two locations. While the model described measured pressure heads and their dynamics very well in the wet range, there were larger differences in the drier range of pressure head values. Since

the retention curves are relatively steep in this range of pressure head values, however, these differences correspond to only small differences in water contents. It should be emphasized that numerical simulations were performed using measured values of soil hydraulic properties without any additional model calibration. Correspondence between measured and simulated drainage fluxes and pressure heads is thus reasonable. Had the numerical model been calibrated (which is, due to significant computational requirements, still a rather difficult task for problems involving three-dimensional transport domains), correspondence between

FIG. 9. Measured and simulated cumulative fluxes from four lysimeters.
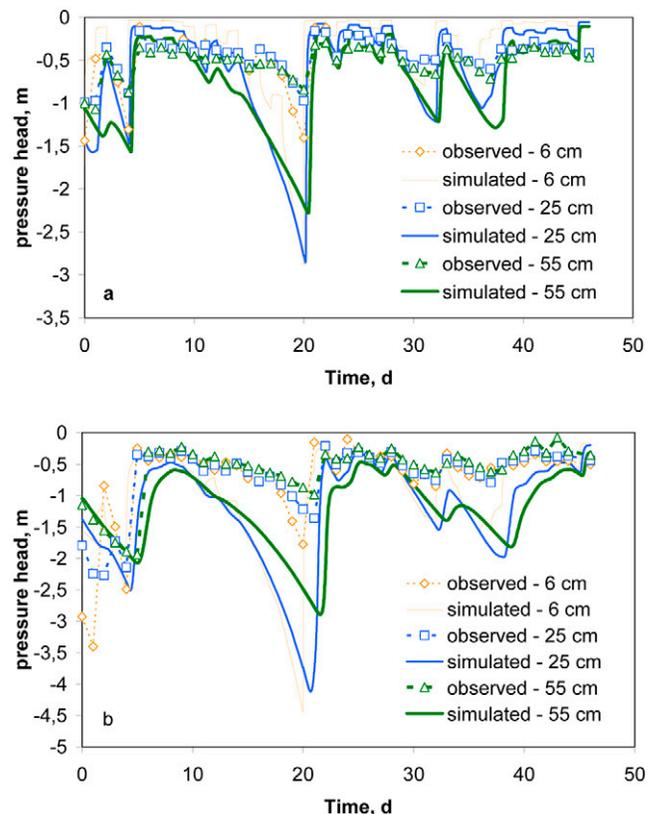
FIG. 10. Measured and simulated pressure heads (a) under the plant stem and (b) between the rows.

measured and simulated values of drainage fluxes and pressure heads would probably have been much better.

Conclusions

The numerical model used in this study reproduced the general trends of distributed measured drainage under a banana plant in an Andisol fairly well. Numerical modeling was probably successful because of the precise determination of the Andisol hydrologic parameters [i.e., the soil water retention curve $\theta(h)$, and the saturated hydraulic conductivity, K_s] by a combination of laboratory and field experiments. Using experimental and calculated drained volumes, as well as soil pressure head data, we attributed drainage fluxes under the banana stem or immediately downstream from the stem almost exclusively to the stemflow. The drained volumes under the banana stem were six times higher than 1.2 m downstream from the stem in the row and between the rows, since both these zones were sheltered by the banana leaves and received essentially only throughfall. Simulations showed that under heavy fluxes, such as those due to stemflow, the wicks reproduced the actual field drainage reasonably well. Under smaller surface fluxes (e.g., throughfall), measured water fluxes with lysimeters were, on average, 50% underestimated compared with simulated water fluxes without lysimeters.

The spatially distributed water fluxes under the banana plant also considerably influence solute transport. Our results, i.e., a concentrated water flow around the plant stem, bring into question the common practice of applying fertilizers and pesticides at the foot of the plant. Under these conditions, the abundant stemflow may rapidly leach the soluble nutrients or pesticides from the root zone into deeper horizons, and eventually into the groundwater. This process will be especially important after flowering, when rainfall interception is maximal. We therefore recommend that additional research be conducted to evaluate how our results can be interpreted in the context of a locally and intensively fertilized banana plantation. Such research could provide better guidelines for fertilization practices that would better protect subsurface water resources.

References

Arya, L.M., G.R. Blake, and D.A. Farrell. 1975. A field study of soil water depletion patterns in presence of growing soybean roots: II. Effect of plant growth on soil water pressure and water loss patterns. Soil Sci. Soc. Am. J. 39:433–436.

Assouline, S. 2002. The effects of microdrip and conventional drip irrigation on water distribution and uptake. Soil Sci. Soc. Am. J. 66:1630–1636.

Bassette, C. 2005. Modélisation 3-D de l'interception de la pluie par le bananier: Effets de caractéristiques physiques du couvert sur les flux d'eau et de d'énergie cinétique de la pluie transmis au sol. Ph.D. diss. Univ. of Antilles-Guyane, Guadeloupe, French West Indies.

Bassette, C., and F. Bussière. 2005. 3-D modelling of the banana architecture for simulation of rainfall interception parameters. Agric. For. Meteorol. 129:95–100.

Boll, J., T.S. Steenhuis, and J.S. Selker. 1992. Fiberglass wicks for sampling of water and solutes in the vadose zone. Soil Sci. Soc. Am. J. 56:701–707.

Carlyle-Moses, D.E., and A.G. Price. 1999. An evaluation of the Gash interception model in a northern hardwood stand. J. Hydrol. 214:103–110.

Cattan, P., M. Voltz, Y.-M. Cabidoche, J.-G. Lacas, and J. Sansoulet. 2007. Spatial and temporal variations in percolation fluxes in a tropical Andosol influenced by banana cropping patterns. J. Hydrol. 335:157–169.

Celia, M.A., E.T. Bouloutas, and R.L. Zarba. 1990. A general mass-conservative numerical solution for the unsaturated flow equation. Water Resour. Res. 26:1483–1496.

Chabot, R., S. Bouarfa, D. Zimmer, C. Chaumont, and C. Duprez. 2002. Sugarcane transpiration with shallow water-table: Sap flow measurements and modelling. Agric. For. Meteorol. 54:17–36.

Feddes, R.A., P.J. Kowalik, and H. Zaradny. 1978. Simulation of field water use and crop yield. John Wiley & Sons, New York.

Godefroy, J., and M. Dormoy. 1988. Mineral fertilizer element dynamics in the "soil–banana–climate" complex. Application to the programming of fertilization: III. The case of Andosols. Fruits 43:263–267.

Herbst, M., W. Fialkiewicz, T. Chen, T. Pütz, D. Thiéry, C. Mouvet, G. Vachaud, and H. Vereecken. 2005. Intercomparison of flow and transport models applied to vertical drainage in cropped lysimeters. Vadose Zone J. 4:240–254.

Jarvis, N. 1991. MACRO: A model of water movement and solute transport in macroporous soils. Rep. Diss. 19. Dep. of Soil Science, Swedish Univ. of Agricultural Science, Uppsala.

Kao, C., S. Bouarfa, and D. Zimmer. 2001. Steady state analysis of unsaturated flow above a shallow water-table aquifer drained by ditches. J. Hydrol. 250:122–133.

Knutson, J.H., and J.S. Selker. 1994. Unsaturated hydraulic conductivities of fiberglass wicks and designing capillary wick pore-water samplers. Soil Sci. Soc. Am. J. 58:721–729.

Lacas, J.G., M. Voltz, and P. Cattan. 2003. Numerical evaluation of passive capillary samplers. Geophys. Res. Abstr. 6:06149.

Lafolie, F. 1991. Modelling water flow, nitrogen transport and root uptake including physical non-equilibrium and optimization of the root water potential. Fert. Res. 27:215–231.

Lecompte, F., H. Ozier-Lafontaine, and L. Pagès. 2003. An analysis of growth rates and directions of growth of primary roots of field-grown banana trees in an Andisol at three levels of soil compaction. Agronomie 23:209–218.

Levia, D.F., Jr., and E.E. Frost. 2003. A review and evaluation of stemflow literature in the hydrologic and biogeochemical cycles of forested and agricultural ecosystems. J. Hydrol. 274:1–29.

Mertens, J., D. Raes, and J. Feyen. 2001. Incorporating rainfall intensity into daily rainfall records for simulating runoff and infiltration into soil profiles. Hydrol. Processes 16:731–739.

Météo France. 2000. Bulletin climatologique annuel. Service Régional de la Guadeloupe, France.

Mohrath, D., L. Bruckler, P. Bertuzzi, J.C. Gaudu, and M. Bourlet. 1997. Error analysis of an evaporation method for determining hydrodynamic properties in unsaturated soil. Soil Sci. Soc. Am. J. 61:725–735.

Monteith, J.L. 1965. Evaporation and environment. p. 205–234. In G.E. Fogg (ed.) The state and movement of water in living organisms. Symp. Soc. Exp. Biol., 19th, Swansea. 8–12 Sept. 1964. Vol. 19. Cambridge Univ. Press, Cambridge, UK.

Mualem, Y. 1976. A new model for predicting the hydraulic conductivity of unsaturated porous media. Water Resour. Res. 12:513–522.

Nash, J.E., and J.V. Sutcliffe. 1970. River flow forecasting through conceptual models: Part I. A discussion of principles. J. Hydrol. 10:282–290.

Ndayiragije, S. 1996. Caractérisation d'une séquence d'altération de sols dérivés de matériaux pyroclastiques sous climat tropical humide des Antilles (Guadeloupe). Ph.D. diss. Université Catholique de Louvain, Louvain, Belgium.

Pang, L., M.E. Close, J.P.C. Watt, and K.W. Vincent. 2000. Simulation of picloram, atrazine, and simazine leaching through two New Zealand soils and into groundwater using HYDRUS-2D. J. Contam. Hydrol. 44:19–46.

Pellerin, S. 1986. Etude d'une série chronologique de rendements de canne à sucre obtenus en Guadeloupe à partir d'un modèle de simulation du bilan hydrique. Agronomie 6:91–98.

Persicani, D., G. Gasparetti, P. Siro, and M. Bonvini. 1995. Measurement and simulation of atrazine and alachlor leaching into two field soils. J. Contam. Hydrol. 19:127–144.

Quantin, P. 1994. The Andosols. p. 848–859. *In* Trans World Congr. of Soil Sci., 15th, Acapulco, Mexico. 10–16 July 1994. Vol. 6a. Sociedad Mexicana de la Ciencia del Suelo, Chapingo, Mexico.

Reynolds, W.D., D.E. Elrick, and E.G. Youngs. 2002. Single-ring and double- or concentric-ring infiltrometers. p. 821–826. *In* J.H. Dane and G.C. Topp (ed.) Methods of soil analysis: Part 4. Physical methods. SSSA Book Ser. 5. SSSA, Madison, WI.

Richards, L.A. 1931. Capillary conduction of liquids through porous media. Physics 1:318–333.

Rimmer, A., T.S. Steenhuis, and J.S. Selker. 1995. One-dimensional model to evaluate the performance of wick samplers in soils. Soil Sci. Soc. Am. J. 59:88–92.

Sansoulet, J., Y.M. Cabidoche, and P. Cattan. 2007. Adsorption and transport of nitrate and potassium in an Andosol under banana (Guadeloupe, French West Indies). Eur. J. Soil Sci. 58:478–489.

Shoji, S., M. Nanzyo, and R. Dahlgren. 1993. Volcanic ash soils: Genesis, properties and utilization. Dev. Soil Sci. 21. Elsevier, Amsterdam.

Šimůnek, J., M.Th. van Genuchten, and M. Šejna. 2006. The HYDRUS software package for simulating two- and three-dimensional movement of water, heat, and multiple solutes in variably saturated media. Technical manual, Version 1.0. PC Progress, Prague, Czech Republic.

Šimůnek, J., O. Wendroth, and M.Th. van Genuchten. 1998. A parameter estimation analysis of the evaporation method for determining soil hydraulic properties. Soil Sci. Soc. Am. J. 62:894–905.

Soil Survey Staff. 1996. Keys to Soil Taxonomy. 7th ed. U.S. Gov. Print. Office, Washington, DC.

Sommer, R., H. Folster, K. Vielhauer, E.J.M. Carvalho, and P.L.G. Vlek. 2003. Deep soil water dynamics and depletion by secondary vegetation in the eastern Amazon. Soil Sci. Soc. Am. J. 67:1672–1686.

Taniguchi, M., M. Tsujimura, and T. Tanaka. 1996. Significance of stemflow in groundwater recharge: 1. Evaluation of the stemflow contribution to recharge using a mass balance approach. Hydrol. Proc. 10:71–80.

Vandervelde, M., S.R. Green, G.W. Gee, M. Vanclooster, and B.E. Clothier. 2005. Evaluation of drainage from passive suction and nonsuction flux meters in a volcanic clay soil under tropical conditions. Vadose Zone J. 4:1201–1209.

van Genuchten, M.Th. 1980. A closed form equation for predicting the hydraulic conductivity of unsaturated soils. Soil Sci. Soc. Am. J. 44:892–898.

Ventrella, D., B.P. Mohanty, J. Šimůnek, N. Losavio, and M.Th. van Genuchten. 2000. Water and chloride transport in a fine-textured soil: Field experiments and modeling. Soil Sci. 165:624–631.

Wind, G.P. 1968. Capillary conductivity data estimated by a simple method. p. 181–191. *In* P.P.E. Rijtema and H. Wassink (ed.) Water in the unsaturated zone. Proc. Wageningen Symp., the Netherlands. 19–25 June 1966. Vol. 1. Publ. 82. Int. Assoc. Scientific Hydrol., Gentbrugge, Belgium.

Young, C.A., and W.W. Wallender. 2002. Spatially distributed irrigation hydrology: Water balance. Trans. ASAE 45:609–618.